Tetrahedron 67 (2011) 7431–7439

Contents lists available at ScienceDirect

Tetrahedron

journal homepage: www.elsevier.com/locate/tet

Twisted molecular geometry and localized electronic structure of the triplet excited *gem*-diphenyltrimethylenemethane biradical: substituent effects on thermoluminescence and related theoretical calculations

Yasunori Matsui [a], Hayato Namai [b], Ikuko Akimoto [c,*], Ken-ichi Kan'no [c], Kazuhiko Mizuno [a,d], Hiroshi Ikeda [a,d,*]

[a] Department of Applied Chemistry, Graduate School of Engineering, Osaka Prefecture University, Sakai, Osaka 599-8531, Japan
[b] Department of Chemistry, Graduate School of Science, Tohoku University, Sendai 980-8578, Japan
[c] Department of Material Science and Chemistry, Faculty of Systems Engineering, Wakayama University, Wakayama 640-8510, Japan
[d] Research Institute for Molecular Electronic Devices (RIMED), Osaka Prefecture University, Sakai, Osaka 599-8531, Japan

ARTICLE INFO

Article history:
Received 30 April 2011
Received in revised form 14 June 2011
Accepted 18 June 2011
Available online 7 July 2011

This paper is dedicated to the memory of Emeritus Professor Yuho Tsuno (Kyushu University)

Keywords:
Hammett equation
Electronic structure
Molecular geometry
Electron transfer
Charge recombination

ABSTRACT

Substituent effects on the energies of electronic transitions (ETs) between the triplet excited and ground states of *gem*-diphenyltrimethylenemethane biradicals (^{3}**2a**••) were explored by using thermoluminescence (TL) spectroscopy and density functional theory (DFT) including time-dependent (TD) DFT. Linear free energy (Hammett) analyses of TL energies of a variety of *para*-substituted aryl derivatives of ^{3}**2**••* gave reasonable correlations with the substituent constant, $\sigma^{\bullet}$. The slope of Hammett plots of the data are nearly identical to one obtained from a similar analysis of the photoluminescence (PL) energies of the structurally-related 1,1-diarylethyl radicals (**3**•*). The results suggest that TL of ^{3}**2**••* and PL of **3**•* derive from a common diarylmethyl radical fluorophore. This interpretation is also supported by the DFT and TDDFT calculated electronic structures and ET energies of ^{3}**2**•• and **3**•. Thermodynamic and kinetic analyses of the charge recombination (CR) process between **2**•$^+$ and **1**•$^-$, which generates ^{3}**2**••*, revealed that substituents not only alter the TL energies but also the TL intensities of ^{3}**2**••*. The observations made in this effort demonstrate that ^{3}**2**••* as well as ^{3}**2**•• and **2**•$^+$ have greatly twisted molecular geometries and highly localized electronic structures.

1. Introduction

Linear free energy relationships, exemplified by the Hammett equation,[1] are perhaps the most fundamentally important tools in physical organic chemistry. Although the Hammett equation was originally based on thermodynamic relationships associated with the acidities of *para*-substituted benzoic acids, and applied to kinetic analyses of reactions, it is also used to probe features of electronic transitions (ETs) of interesting molecules or intermediates. Studies of substituent effects on ETs associated with light absorption and emission can provide information about electronic structures, molecular geometries, reactivities, and other properties of the excited states of molecules.[2] Hammett analyses that utilize substances containing electron-donating (EDGs) and/or electron-withdrawing groups (EWGs) is a sophisticated strategy for this purpose.

Substituent effects on short-lived organic radicals[3] also have been studied both theoretically[4] and experimentally[5,6] to analyze reaction mechanisms, especially in the context of materials chemistry.[7] As compared with closed-shell molecules, organic radicals have some advantages, such as ideal reversible redox properties and low energy (i.e., longer wavelength) ETs caused by the presence of characteristic SOMO energy levels that exist between HOMOs and LUMOs.

Thus, organic radicals hold great potential in the fields of organic electronic devices, such as photovoltaics,[8] batteries,[9] and light-emitting diodes (OLEDs).[10] Unfortunately, few studies aimed at exploring the substituent effects on ET energies of organic radicals have been carried out.

Previously, we described the observation of an intense green (λ_{TL}=501 nm) thermoluminescence (TL) during annealing of γ-[10a] or X-irradiated[10c] methylcyclohexane (MCH) matrices containing 2,2-diphenyl-1-methylenecyclopropane (**1a**, Scheme 1).[10] The TL was assigned to fluorescence associated with decay of the triplet excited state of the *gem*-diphenyltrimethylenemethane biradical (^{3}**2a**••*) to

* Corresponding authors. E-mail addresses: akimoto@sys.wakayama-u.ac.jp (I. Akimoto), ikeda@chem.osakafu-u.ac.jp (H. Ikeda).

0040-4020/$ – see front matter © 2011 Elsevier Ltd. All rights reserved.
doi:10.1016/j.tet.2011.06.052

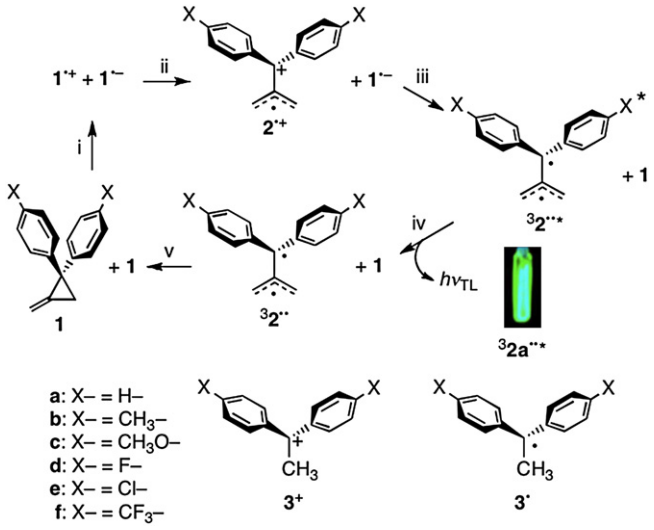

Scheme 1. Mechanism for TL emission from ^{3}**2**••* (photo: ^{3}**2a**••*): (i) charge separation induced by γ- or X-irradiation, (ii) bond fission, (iii) CR between **2**•$^+$ and **1**•$^-$ on annealing, (iv) deactivation accompanied by TL (fluorescence), (v) regeneration of **1** by bond formation.

its triplet ground state. In this report, we proposed a new OLED strategy utilizing ^{3}**2**••* as an emitter, which we named *Organic Radical Light-Emitting Diode* (*ORLED*), and suggested that this approach has great potential for overcoming significant problems associated with normal fluorescent emitters used in typical OLEDs.[10a] TL and electroluminescence (EL) of ^{3}**2**••* are induced by charge recombination (CR) between **2**•$^+$ and a radical anion of **1** (**1**•$^-$) and an electron (e^-), respectively. UV–vis absorption spectroscopic studies of **2**•$^+$ and structurally-related 1,1-diarylethyl cations (**3**$^+$, Scheme 1) by Ikeda and co-workers[11] revealed that **2**•$^+$ have a unique, largely twisted molecular geometry and separated electronic structure containing isolated radical and cation centers.

To develop ORLEDs using the **1a**/^{3}**2a**••* system, studies of substituent effects on the ETs of ^{3}**2**•• and ^{3}**2**••* are important so that their molecular geometries and electronic structures can be clarified. For this purpose, we have carried out an investigation in which substituent effects on TL energy of ^{3}**2**••* were examined by employing derivatives ^{3}**2b**–**f**••* that bear CH_3, CH_3O, F, Cl, and CF_3 groups on the C4 positions of two benzene rings. The photoluminescence (PL) energies of the structurally-related **3a**–**f**•* were also investigated. Finally, DFT and TDDFT calculations on ^{3}**2a**–**f**•• and **3a**–**f**• were performed. Below, we present the results of this effort, which show that ^{3}**2**••* possess twisted molecular geometries and separated electronic structures and provide the basis for thermodynamic and kinetic analyses of the CR process between **2**•$^+$ and **1**•$^-$.

2. Experimental section

2.1. General methods

All melting points were obtained with a Yanako (MP-500) apparatus and are reported uncorrected. Satisfactory elemental analyses were obtained for a new compound, **1f**. ^{1}H NMR spectra were recorded at 300 MHz ^{13}C NMR spectra were obtained at 75 MHz. MCH (spectroscopic grade) was dried over molecular sieves 4 Å. Other solvents used for syntheses were purified and dried by usual methods.

2.2. Preparation of substrates

Physical data of **1a**–**e** are reported in Ref. 11a, while those of 2,2-bis(4′-trifluoromethylphenyl)-1-methylenecyclopropane (**1f**) are as follows: colorless needles from ethanol (mp 49–50 °C); ^{1}H NMR (300 MHz, $CDCl_3$) δ_{ppm} 1.99 (2H, dd, J=2.7, 2.0 Hz), 5.69 (1H, td, J=2.3, 2.0 Hz), 5.84 (1H, td, J=2.7, 2.3 Hz), 7.36 (4H, AA′BB′, J=8.2 Hz), 7.55 (4H, AA′BB′, J=8.2 Hz); ^{13}C NMR (75 MHz, $CDCl_3$) δ_{ppm} 22.3, 32.8, 105.5, 122.3, 125.3 (q, 2C), 128.2 (4C), 128.4 (4C), 137.6 (2C), 146.6 (2C); IR (KBr) 1616, 1325, 1163, 1117, 1069, 1013, 901, 858 cm^{-1}; Anal. Calcd for $C_{18}H_{12}F_6$: C 63.16, H 3.53, F 33.30, found: C 63.45, H 3.78, F 33.56.

2.3. TL of ^{3}2••* induced by using the γ-irradiation–annealing method

A solution of MCH (1 mL) containing **1** (5 mM) in a flat vessel [suprasil, 2×10×40 mm] was degassed by using five freeze (77 K)–pump (0.1 mmHg)–thaw (room temperature) cycles. After sealing the tube, a glassy MCH matrix was prepared by immersion in a Dewar vessel filled with liquid nitrogen. γ-Irradiation was carried out with 4.0 TBq ^{60}Co source in liquid nitrogen at 77 K for 40 h at Tohoku University. The matrix was rapidly annealed at room temperature. TL spectra during the annealing process were recorded by using the photonic multichannel spectral analyzer (PMA-11, Hamamatsu Photonics).

2.4. TL of ^{3}2••* induced by using the X-irradiation–annealing method[12]

A solution of MCH (0.1 mL) containing **1** (20 mM) in a quartz ESR tube (ϕ=5 mm) was degassed by using five freeze (77 K)–pump (0.1 mmHg)–thaw (room temperature) cycles. After sealing the tube, a glassy MCH matrix was prepared by immersion in a quartz Dewar vessel filled with liquid nitrogen. X-Irradiation (40 kV, 1 mA) was carried out by using equipment consisting of an X-ray tube (Oxford, Series 5000/75, W target, λ_{MAX}=0.05 nm) and power supply (SPELLMAN, XLG). The matrix was annealed slowly in the same Dewar vessel. TL spectra during annealing process were recorded at 2 s intervals with an exposure time of 2 s by using a CCD detector (Roper Scientific, Spec-10: 256TE-A) and spectrofluorometer (Acton Research Corp., Spectrapro-150i). Temperature monitoring of the matrix was carried out with a Au:Fe–Chromel thermocouple.

2.5. PL of 3•*

The 1,1-diarylethyl radical derivatives **3a**–**f**• were generated by γ-irradiation (40 h, 4.0 TBq) of the degassed glassy MCH matrices containing the corresponding 1,1-diarylethanol (**4a**–**f**, Scheme 2) in the quartz vessels at 77 K. PL spectra of **3a**–**f**•* were then recorded by using PMA-11 on photoexcitation (λ_{EX}∼340 nm) at 77 K.

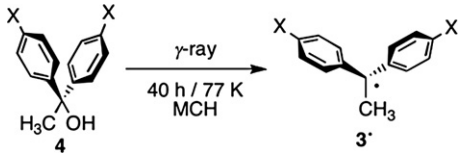

Scheme 2. Generation of the 1,1-diarylethyl radicals (**3**•).

2.6. Quantum chemical calculations

Geometry optimizations of ^{3}**2**•• and **3**• were performed with the cc-pVDZ basis set,[13] using UB3LYP method.[14,15] ETs were computed using the TD-UB3LYP method[16] with cc-pVDZ basis set. Spin contaminations are negligible. All the calculations were performed on Gaussian 98 program.[18]

In this effort, ab initio MO calculations, such as those using the second-order Møller–Plesset (MP2) method, were not carried out because overestimation of spin densities and spin contaminations often occur in case of open-shell species. In contrast, DFT methods often give more satisfactory results for these species. Stephens and co-workers reported that compared with the self-consistent field or MP, DFT/B3LYP accurately predicts vibrational absorption and circular dichromism spectra.[19] Our experience also shows that the DFT method is sufficiently accurate to give reliable molecular geometries and electronic structures of **2**$^{\bullet+}$ (UB3LYP/cc-pVDZ)[11] and the 1,4-diarylcyclohexane-1,4-diyl radical cations (UB3LYP/cc-pVDZ),[20] as well as other species.

3. Results and discussion

3.1. Time-dependent TL spectra

A γ-irradiated MCH matrix containing **1a** in a flat vessel (2×10×40 mm) was annealed at a rate of ca. 70 K min^{-1} until the melting point of MCH (147 K[21]) was reached (within ca. 50 s). Emission spectra associated with TL, observed during the course of the annealing process, are shown in Fig. 1a. TL, which began at the early stage of annealing (t_A=30 s) and was complete by t_A=80 s, displayed bands with maxima at λ_{TL}=501 and 533 nm. The bands are assigned to T–T fluorescence of ^{3}**2a**$^{\bullet\bullet}$*.[10] TL emission spectra of an X-irradiated MCH matrix containing **1a** in an ESR tube (ϕ=5 mm) during annealing are displayed in Fig. 1b. TL in this case, where the matrix was slowly annealed (ca. 20 K min^{-1}) in the Dewar vessel, began relatively slowly (t_A=90 s) and finished at t_A=170 s, as compared to when the γ-irradiation method was employed.

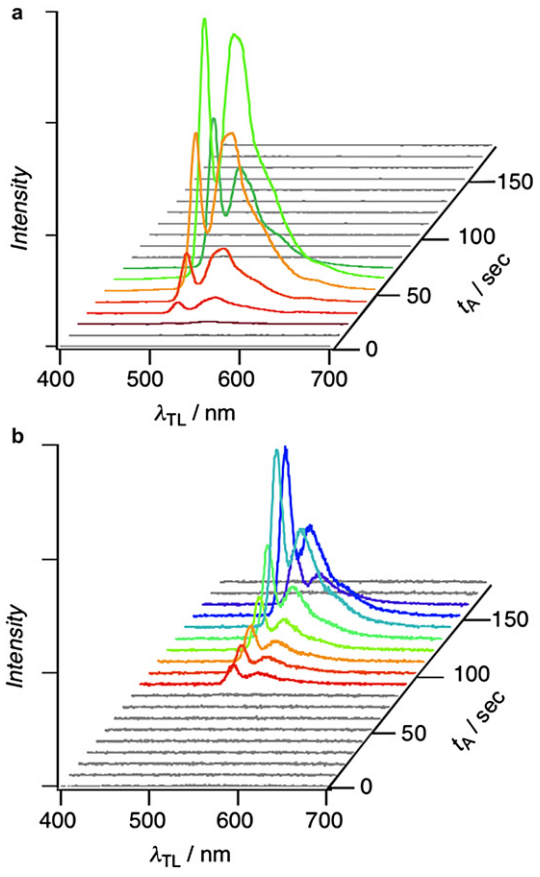

Fig. 1. Time-dependent changes of TL spectra of ^{3}**2a**$^{\bullet\bullet}$* in (a) γ-irradiated and (b) X-irradiated MCH matrices obtained every 10 s following t_A=0.

TL spectra obtained under γ-irradiation conditions were relatively broad, as compared with those under X-irradiation conditions. Annealing of the γ-irradiated matrix in a flat vessel results in altered shape of emission band at ca. 540 nm (Fig. 1a) that results from the existence of a range of conformers of ^{3}**2a**$^{\bullet\bullet}$* owing to the wide temperature distribution in the relatively large flat vessel and the fast rate of annealing. In contrast, when X-irradiation conditions are used, annealing does not result in a change of the shape of TL bands since only a few conformers of ^{3}**2a**$^{\bullet\bullet}$* owing to the narrow temperature distribution in the relatively small ESR tube and the slow rate of annealing. Unfortunately, however, a direct comparison is not possible due to the characteristics of radiation sources that a γ-ray radiates from the source (^{60}Co) in a radial fashion, while a source of XRD equipment radiates X-ray in a small range (ϕ=5 mm). Thus, the flat vessel and ESR tube are suitable for γ- and X-irradiation, respectively.

Although the γ- and X-rays have respective high (2.8 MeV) and low (ca. 1 keV) photon energies, the same phenomenon (i.e., ionization of substrates followed by TL emission) occurs. Note that photon energies or ionizing power to finally produce ^{3}**2a**$^{\bullet\bullet}$* does not affect on TL wavelengths. Consequently, the differences in the shapes of bands in the TL spectra coming from annealing γ- and X-irradiated samples appear to be caused by differences in the shapes of the vessels and the annealing environments.

3.2. Hammett analysis of TL energies of ^{3}2$^{\bullet\bullet}$*

Annealing of γ-irradiated glassy MCH matrices containing **1a**–**f** from 77 K to ca. 147 K give rise to emission spectra with TL bands at $\lambda_{TL}(\gamma)$=501, 515, 529,[22] 503, 525, and 515 nm, respectively [Fig. 2a–f (green), Table 1]. Similarly, annealing of X-irradiated glassy MCH matrices containing these substances from 77 K to ca. 147 K yields spectra with TL bands at $\lambda_{TL}(X)$=501, 514, 503, 521, and 515 nm, respectively [Fig. 2a–f (blue), Table 1]. Under the X-irradiation conditions, the halogenated derivatives **1d** and **1e** were found to exhibit very weak TL [Fig. 2d and e (blue)]. Moreover, no TL was observed for an X-irradiated matrix containing **1c**. Therefore, Hammett analyses (see below) were performed by using TL energies of ^{3}**2**$^{\bullet\bullet}$* obtained employing the γ-irradiation method.

Although a variety of substituent constants ($\sigma^{\bullet}$) have been defined for radical reactions, $\sigma^{\bullet}$ for diarylmethyl radical moieties or excited states of radicals have not yet been proposed. As a result, we have used the three representative $\sigma^{\bullet}$ parameters that are independently defined by Cheng,[4] Arnold,[5] and Creary[6] for the monoaryl-substituted radicals or related compounds (Table 1). Cheng derived $\sigma^{\bullet}$ (Cheng) constants based on DFT-calculated spin densities (ρ_X) of the benzylic carbon of *para*-substituted benzyl radicals (**5**$^{\bullet}$, Scheme 3a).[4] By using ESR hyperfine coupling constants (α_X) of the two benzylic hydrogen atoms of **5**$^{\bullet}$, Arnold derived $\sigma^{\bullet}$ (Arnold) (Scheme 3b).[5] Finally, Creary derived $\sigma^{\bullet}$ (Creary) by using rate constants (k_X) of the methylenecyclopropane rearrangement of 2-aryl-3,3-dimethyl-1-methylenecyclopropanes (**6**, Scheme 3c) that take place via transition states **7**‡ and trimethylenemethane (TMM)-type intermediates **8**$^{\bullet\bullet}$.[6]

From analyses of TL spectra, recorded upon annealing following γ-irradiation, the relative emission energies of ^{3}**2b**–**f**$^{\bullet\bullet}$* were determined based on $\Delta E_{TL}(^3\mathbf{2}^{\bullet\bullet}{}^*)=E_{TL}(^3\mathbf{2b}\text{–}\mathbf{f}^{\bullet\bullet}{}^*)-E_{TL}(^3\mathbf{2a}^{\bullet\bullet}{}^*)$. These values display a reasonable correlation [correlation coefficient R^2=0.93, see Fig. 3a (solid line) and Eq. 1a] with $\sigma^{\bullet}$ (Cheng). As described below, the PL energy data of the CH$_3$O-substituted derivative of the structurally-related 1,1-diarylethyl radicals (**3c**$^{\bullet}$*, Scheme 1) deviated from the fitted line (Fig. 3d). However, the energies of the corresponding species ^{3}**2c**$^{\bullet\bullet}$* [$\Delta E_{TL}(^3\mathbf{2c}^{\bullet\bullet}{}^*)$] did not. Even when $\Delta E_{TL}(^3\mathbf{2c}^{\bullet\bullet}{}^*)$ is excluded from the analysis, the correlation between $\Delta E_{TL}(^3\mathbf{2}^{\bullet\bullet}{}^*)$ and $\sigma^{\bullet}$ (Cheng) does not significantly change [see Fig. 3a (dotted line) and Eq. 1b]. On the other hand, the fits of $\Delta E_{TL}(^3\mathbf{2}^{\bullet\bullet}{}^*)$ using the other substituent constants, $\sigma^{\bullet}$ (Arnold)

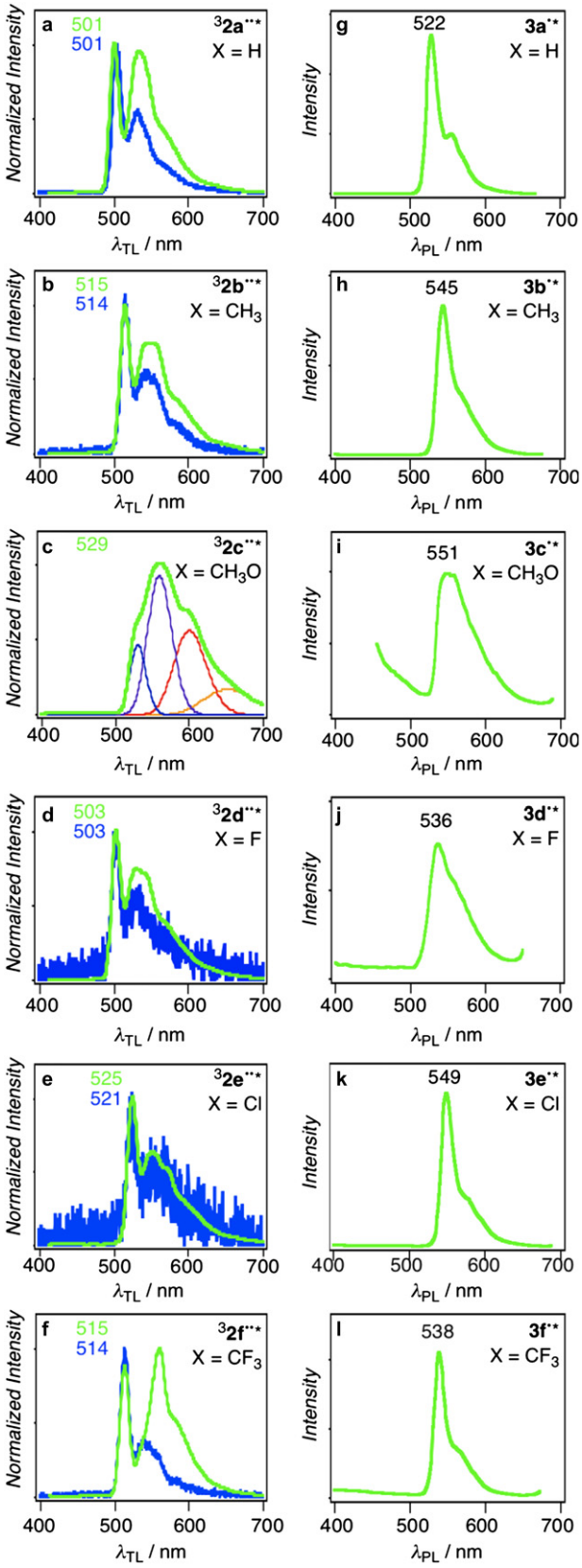

Fig. 2. (a–f) TL spectra of ^{3}**2a**–**f**$^{\bullet\bullet*}$ induced by γ-(green, 40 h at 77 K) and X-irradiation (blue, 1 h at 77 K) of MCH matrices containing **1a**–**f**.[22] (g–l) PL spectra of **3a**–**f**$^{\bullet*}$ in MCH matrices at 77 K, each excitation wavelengths is λ_{EX}=340±10 nm.

Table 1
Substituent constants $\sigma^{\bullet}$, TL, and PL wavelengths of ^{3}**2**$^{\bullet\bullet*}$ and **3**$^{\bullet*}$, and calculated ET wavelengths of ^{3}**2**$^{\bullet\bullet}$ and **3**$^{\bullet}$

X	$\sigma^{\bullet}$ (Cheng)[a]	$\sigma^{\bullet}$ (Arnold)[a]	$\sigma^{\bullet}$ (Creary)[a]	^{3}**2**$^{\bullet\bullet*}$		^{3}**2**$^{\bullet\bullet}$	**3**$^{\bullet*}$	**3**$^{\bullet}$
				λ_{TL} (γ)[b] nm	λ_{TL} (X)[b] nm	λ_{ET}[c] nm	λ_{PL}[d] nm	λ_{ET}[c] nm
H	0.00	0.000	0.00	501	501	412	522	429
CH_3	+0.11	+0.002	+0.16	515	514	423	545	444
CH_3O	+0.22	+0.018	+0.27	529	—[e]	435	551	459
F	+0.03	−0.011	−0.06	503	503	413	536	432
Cl	+0.14	+0.011	+0.11	525	521	431	549	449
CF_3	+0.08	−0.009	+0.05	515	515	429	538	446

[a] $\sigma^{\bullet}$ (Cheng), $\sigma^{\bullet}$ (Arnold), and $\sigma^{\bullet}$ (Creary) values are quoted from Refs. 4–6, respectively.
[b] Recorded during annealing of MCH matrices.
[c] Calculated at the TD-UB3LYP/cc-pVDZ level.
[d] Recorded in MCH matrices at 77 K, each excitation wavelength is 340±10 nm.
[e] Not obtained.

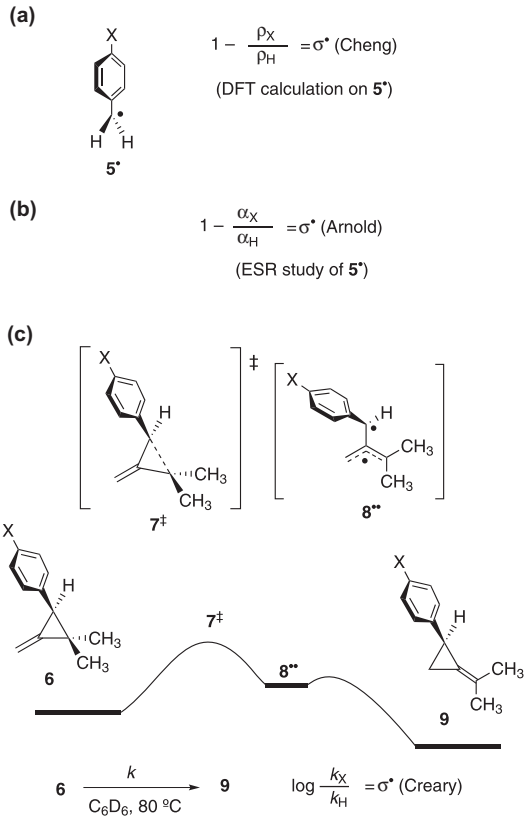

Scheme 3. Species and reactions for definitions of the substituent constants by (a) $\sigma^{\bullet}$ (Cheng) defined with the spin densities (ρ_X) at benzylic carbon of **5**$^{\bullet}$ calculated by DFT, (b) $\sigma^{\bullet}$ (Arnold) defined with ESR hyperfine coupling constants (α_X) of the two benzylic hydrogen atoms of **5**$^{\bullet}$, (c) $\sigma^{\bullet}$ (Creary) defined with the rate constants (k_X) of methylenecyclopropane rearrangements of **6**.

and $\sigma^{\bullet}$ (Creary), are poor (R^2=0.60 and 0.75, see Fig. 3b and c and Eqs. 2 and 3).

$$\Delta E_{TL}(^3\mathbf{2}^{\bullet\bullet*}) = -14.8\sigma^{\bullet}(\text{Cheng}) - 0.06,\ R^2 = 0.93 \quad (1a)$$

$$\Delta E_{TL}(^3\mathbf{2}^{\bullet\bullet*}) = -14.4\sigma^{\bullet}(\text{Cheng}) - 0.17,\ R^2 = 0.93 \quad (1b)$$

$$\Delta E_{TL}(^3\mathbf{2}^{\bullet\bullet*}) = -84.4\sigma^{\bullet}(\text{Arnold}) - 1.33,\ R^2 = 0.60 \quad (2)$$

$$\Delta E_{TL}(^3\mathbf{2}^{\bullet\bullet*}) = -8.91\sigma^{\bullet}(\text{Creary}) - 0.70,\ R^2 = 0.75 \quad (3)$$

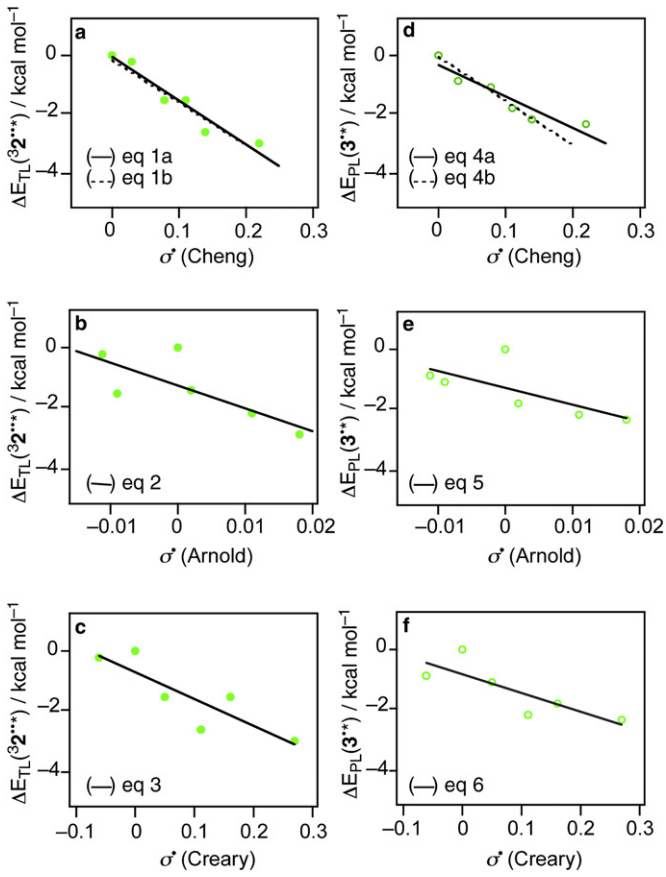

Fig. 3. Hammett plots of TL energies of ^{3}**2a**–**f**$^{\bullet\bullet}$* [$\Delta E_{TL}(^3$**2**$^{\bullet\bullet}$*)] obtained under γ-irradiation–annealing conditions (green dots) against (a) $\sigma^\bullet$ (Cheng), (b) $\sigma^\bullet$ (Arnold), and (c) $\sigma^\bullet$ (Creary) and of PL energies of **3a**–**f**$^\bullet$* [ΔE_{PL}(**3**$^\bullet$*)] (green circles) in MCH matrices at 77 K against (d) $\sigma^\bullet$ (Cheng), (e) $\sigma^\bullet$ (Arnold), and (f) $\sigma^\bullet$ (Creary). Solid fitted lines are obtained by inclusion of data for ^{3}**2a**–**f**$^{\bullet\bullet}$* and **3a**–**f**$^\bullet$* while dotted lines are obtained by exclusion of data for ^{3}**2c**$^{\bullet\bullet}$* and **3c**$^\bullet$*.

It is interesting that $\Delta E_{TL}(^3$**2**$^{\bullet\bullet}$*) correlates with $\sigma^\bullet$ (Cheng) but not with $\sigma^\bullet$ (Arnold) even though these substituent constants originate from analysis of the same benzylic radical **5**$^\bullet$. A possible reason why the TL energies of ^{3}**2**$^{\bullet\bullet}$* do not correlate with $\sigma^\bullet$ (Creary) could lie in the fact that $\sigma^\bullet$ (Creary) comes from a kinetic (or dynamic) analysis, which pertains to the transition states **7**‡ and not biradical intermediates **8**$^{\bullet\bullet}$ involved in the rate determining step of the methylenecyclopropane rearrangement of **6** to give **9** (Scheme 3c).

PL spectra of **3a**–**f**$^\bullet$* in MCH matrices at 77 K are shown in Fig. 2g–l. The radicals **3a**$^\bullet$*, **3b**$^\bullet$*, **3c**$^\bullet$*, **3d**$^\bullet$*, **3e**$^\bullet$*, and **3f**$^\bullet$* exhibited PL bands at λ_{PL}=522, 545, 551, 536, 549, and 538 nm, respectively (Table 1). The relative PL energies of **3b**–**f**$^\bullet$* based on **3a**$^\bullet$* display a reasonable but not good correlation (R^2=0.80) with $\sigma^\bullet$ (Cheng) [see Fig. 3d (solid line) and Eq. 4a]. A decrease in the correlation coefficients R^2 occurs when the data for the CH_3O-substituted derivative **3c**$^\bullet$* is included (Fig. 3d). When the data for **3c**$^\bullet$* is excluded from the analysis, a satisfactory correlation coefficients (R^2=0.97) for ΔE_{PL}(**3**$^\bullet$*) against $\sigma^\bullet$ (Cheng) is obtained [see Fig. 3d (dotted line) and Eq. 4b]. Similar to the analysis of $\Delta E_{TL}(^3$**2**$^{\bullet\bullet}$*), plots of ΔE_{PL}(**3**$^\bullet$*) versus $\sigma^\bullet$ (Arnold) and $\sigma^\bullet$ (Creary) are scattered and poor correlations (R^2=0.47 and 0.67) are observed (see Fig. 3e and f and Eqs. 5 and 6). These results showed that PL characteristics of **3a**–**f**$^\bullet$* are similar to TLs of ^{3}**2a**–**f**$^{\bullet\bullet}$*.

$$\Delta E_{PL}(\mathbf{3}^{\bullet *}) = -10.5\sigma^\bullet(\text{Cheng}) - 0.37,\ R^2 = 0.80 \quad (4a)$$

$$\Delta E_{PL}(\mathbf{3}^{\bullet *}) = -14.9\sigma^\bullet(\text{Cheng}) - 0.10,\ R^2 = 0.97 \quad (4b)$$

$$\Delta E_{PL}(\mathbf{3}^{\bullet *}) = -55.0\sigma^\bullet(\text{Arnold}) - 1.29,\ R^2 = 0.47 \quad (5)$$

$$\Delta E_{PL}(\mathbf{3}^{\bullet *}) = -6.11\sigma^\bullet(\text{Creary}) - 0.85,\ R^2 = 0.67 \quad (6)$$

The relatively large ratio of ρ values for ^{3}**2**$^{\bullet\bullet}$* and **3**$^\bullet$* [$\rho(^3$**2**$^{\bullet\bullet}$*)/ρ(**3**$^\bullet$*)=1.38] suggests that differences exist in the substituent effects on the TL and PL energies of ^{3}**2**$^{\bullet\bullet}$* and **3**$^\bullet$*, respectively. However, the PL energy of **3c**$^\bullet$* deviates significantly from the line obtained from other derivatives [see Fig. 3d and Eq. 4b]. If the data for ^{3}**2c**$^{\bullet\bullet}$* and **3c**$^\bullet$* are excluded from the analysis, the ratio of ρ values is close to unity [$\rho(^3$**2**$^{\bullet\bullet}$*)/ρ(**3**$^\bullet$*)=0.97], demonstrating that almost the same effects of substituents are involved in the TL and PL energies of ^{3}**2**$^{\bullet\bullet}$* and **3**$^\bullet$*, respectively. In other words, little interaction occurs between the diarylmethyl and the allyl radical moieties of ^{3}**2**$^{\bullet\bullet}$*. This result is understandable from the standpoint of the dihedral angle between the diarylmethyl and the allyl moieties of ^{3}**2**$^{\bullet\bullet}$, which is calculated to be smaller than that of the corresponding radical cation **2**$^{\bullet+}$ (see below). Note that Hammett analysis on **2**$^{\bullet+}$ and **3**$^+$ give the ratio ρ(**2**$^{\bullet+}$)/ρ(**3**$^{\bullet+}$)=0.9,[11a] suggesting that **2**$^{\bullet+}$ has a largely-twisted molecular geometry and strongly-separated electronic structure.

In a previous effort probing substituent effects on the TL energies of the singlet excited state of the 1,4-diphenylcyclohexane-1,4-diyl (^{1}**10**$^{\bullet\bullet}$*, Chart 1),[23] we observed that $\Delta E_{TL}(^1$**10**$^{\bullet\bullet}$*) displays a reasonable correlation with $\sigma^\bullet$ (Arnold) but not with $\sigma^\bullet$ (Cheng) and $\sigma^\bullet$ (Creary). The excited biradicals ^{3}**2**$^{\bullet\bullet}$* and ^{1}**10**$^{\bullet\bullet}$* share a common benzyl radical, yet their ET energies are well correlated with different constants, $\sigma^\bullet$ (Cheng) and σ (Arnold), respectively. The multiplicities of biradicals (triplet or singlet), nature of orbital interaction between the two radical moieties,[24] and/or charge-transfer character of the excited states may be the cause(s) of these differences.

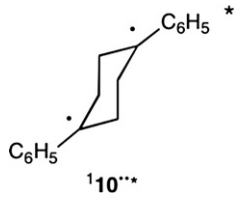

Chart 1. The singlet excited state of the 1,4-diphenylcyclohexane-1,4-diyl (^{1}**10**$^{\bullet\bullet}$*).

3.3. DFT calculations of the molecular geometries and electronic structures of ^{3}**2**$^{\bullet\bullet}$

Quantum chemical studies of the molecular geometries and electronic structures of ^{3}**2**$^{\bullet\bullet}$* are essential to develop an understanding of TL. In general, however, it is difficult to evaluate accurately the properties of excited states of open-shell species, such as ^{3}**2**$^{\bullet\bullet}$*. Thus, DFT and TDDFT calculations were performed on ^{3}**2a**–**f**$^{\bullet\bullet}$ and **3a**–**f**$^\bullet$ to gain information about the TL of ^{3}**2**$^{\bullet\bullet}$*.

The optimized molecular geometry of the parent ^{3}**2a**$^{\bullet\bullet}$ is displayed in Fig. 4. The bond lengths, dihedral angles, spin (ρ) and charge (q) densities of ^{3}**2a**–**f**$^{\bullet\bullet}$, calculated with UB3LYP/cc-pVDZ, are listed in Table 2. All C1–C2 bond lengths (l, Table 2) of

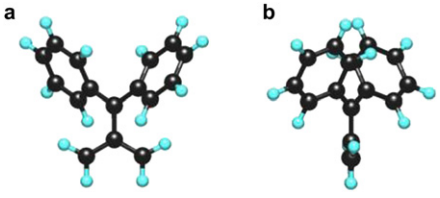

Fig. 4. (a) Front and (b) side views of optimized molecular geometry of ^{3}**2a**$^{\bullet\bullet}$ at UB3LYP/cc-pVDZ level.[10c,25]

Table 2
Bond lengths (l), dihedral angles (θ, ω), and spins ($\Sigma\rho$) and charge distributions (Σq) in the diarylmethyl (subunit I) and allyl (subunit V) moieties of ^{3}**2a**–**f**•• (UB3LYP/cc-pVDZ)[26]

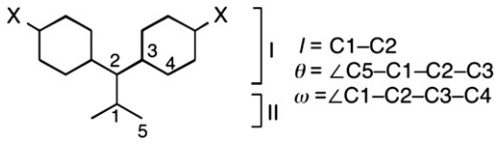

Biradicals	X	Subunit I		Subunit II		l Å	θ deg	ω deg
		$\Sigma\rho$	Σq	$\Sigma\rho$	Σq			
^{3}**2a**••	H	+0.892	+0.018	+1.108	−0.018	1.468	32.2	36.0
^{3}**2b**••	CH_3	+0.895	+0.028	+1.105	−0.028	1.469	33.0	35.2
^{3}**2c**••	CH_3O	+0.891	+0.048	+1.109	−0.048	1.468	32.3	35.5
^{3}**2d**••	F	+0.892	+0.019	+1.108	−0.019	1.468	32.5	35.9
^{3}**2e**••	Cl	+0.899	+0.019	+1.101	−0.019	1.470	33.7	35.0
^{3}**2f**••	CF_3	+0.901	−0.005	+1.099	+0.005	1.471	34.0	34.8

^{3}**2a**–**f**•• were found to be in the range of 1.468–1.471 Å. Dihedral angles between the diarylmethyl and allyl moieties (θ=∠C5–C1–C2–C3) and between the TMM and phenyl moieties (ω=∠C1–C2–C3–C4) of ^{3}**2a**–**f**•• are in the range of θ=32.2–34.0° and ω=34.8–35.9°, respectively. Thus, no clear correlation exists between geometries (l, θ, ω) and substituents. On the other hand, the CH_3- and CH_3O-derivatives ^{3}**2b**•• and ^{3}**2c**•• possess greater positive charge densities in the diarylmethyl moieties (subunit I, Σq=+0.028 for ^{3}**2b**••, +0.048 for ^{3}**2c**••) as compared with ^{3}**2a**•• (Σq=+0.018). Conversely, the CF_3-derivative ^{3}**2f**•• has negative charge density (Σq=−0.005 for ^{3}**2f**••) in the subunit I in contrast to ^{3}**2a**••. Interestingly, as compared to ^{3}**2a**••, the F- and Cl-derivatives ^{3}**2d**•• and ^{3}**2e**•• have slightly greater positive charges (Σq=+0.019 for ^{3}**2d**•• and ^{3}**2e**••) in the subunit I, suggesting that the halogens participate as weak EDGs. Therefore, the observed changes seen in the charge distributions in the subunit I are reasonable from the standpoint of the electron-donating and -withdrawing abilities of the substituents.

In contrast to the observations summarized above, the spin densities in subunit I of ^{3}**2a**–**f**•• fall in the narrow range of $\Sigma\rho$=0.891–0.901, showing that no remarkable substituent effects take place. In addition, these values show that one of the spins of biradical is localized in subunit I and the other is localized in the allyl moieties (subunit II). Thus, the electronic structures contain isolated subunits I and II. Consequently, introduction of EDGs and EWGs into the phenyl groups of ^{3}**2a**•• does not significantly change spin densities and, therefore, the major electronic properties of ^{3}**2a**•• are retained in ^{3}**2b**–**f**••.

3.4. Hammett plots of TDDFT calculated ET energies

The ETs of ^{3}**2a**–**f**••, calculated with TD-UB3LYP/cc-pVDZ, are shown in Table 1. The long wavelengths ETs of ^{3}**2a**••, ^{3}**2b**••, ^{3}**2c**••, ^{3}**2d**••, ^{3}**2e**••, and ^{3}**2f**•• at λ_{ET}=412, 423, 435, 413, 431, and 429 nm, respectively, correspond to transitions of triplet ground states to lowest triplet excited states (^{3}**2**••→^{3}**2**••*). Thus, the transitions are associated with the T–T fluorescence (^{3}**2**••*→^{3}**2**••). Similarly, the wavelengths for the ETs of **3a**•, **3b**•, **3c**•, **3d**•, **3e**•, and **3f**• at λ_{ET}=429, 444, 459, 432, 449, and 446 nm, respectively, corresponds to transitions of doublet ground states to doublet lowest excited states (**3**•→**3**•*) and associated with fluorescence (**3**•*→**3**•). As previously reported, ETs for ^{3}**2a**•• and **3a**• at 412 and 429 nm, respectively, originate from SOMO–LUMO transitions.[10c]

ΔE_{ET} values for ^{3}**2**•• were observed to display a reasonable correlation (R^2=0.80) with σ• (Cheng) even when the ET of ^{3}**2c**•• is excluded from the analysis (R^2=0.80) [see Fig. 5a (solid and dotted lines) and Eqs. 7a and b]. In a similar manner, the calculated ΔE_{ET}(**3**•) values satisfactory correlate (R^2=0.95) with σ• (Cheng)

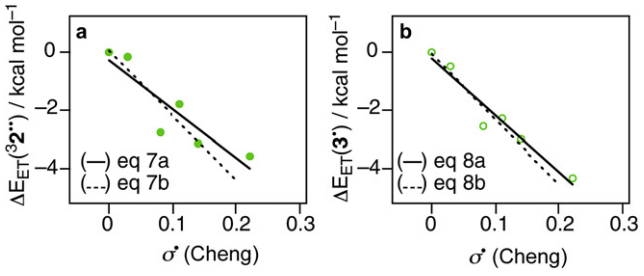

Fig. 5. Hammett plots of the calculated ETs of (a) ^{3}**2a**–**f**•• and (b) **3a**–**f**• calculated at the TD-UB3LYP/cc-pVDZ level versus σ• (Cheng). Solid fitted lines are obtained by inclusion of data for ^{3}**2a**–**f**••* and **3a**–**f**•* while dotted lines are obtained by exclusion of data for ^{3}**2c**••* and **3c**•*.

even when the ET of **3c**• is excluded from the analysis (R^2=0.92) [see Fig. 5b (solid and dotted lines) and Eqs. 8a and 8b].

$$\Delta E_{ET}(^3\mathbf{2}^{\bullet\bullet}) = -17.3\sigma^{\bullet}(\text{Cheng}) - 0.22,\ R^2 = 0.80 \quad (7a)$$

$$\Delta E_{ET}(^3\mathbf{2}^{\bullet\bullet}) = -22.2\sigma^{\bullet}(\text{Cheng}) + 0.06,\ R^2 = 0.80 \quad (7b)$$

$$\Delta E_{ET}(\mathbf{3}^{\bullet}) = -19.6\sigma^{\bullet}(\text{Cheng}) - 0.19,\ R^2 = 0.95 \quad (8a)$$

$$\Delta E_{ET}(\mathbf{3}^{\bullet}) = -22.6\sigma^{\bullet}(\text{Cheng}) - 0.06,\ R^2 = 0.92 \quad (8b)$$

Analyses of the ratio of the slopes of Eqs. 7a and 8a [$\rho(^3\mathbf{2}^{\bullet\bullet})/\rho(\mathbf{3}^{\bullet})$=0.87] suggest that substituents effect the ETs of ^{3}**2**•• and **3**• to nearly the same extent. This conclusion is strongly supported by the ratio $\rho(^3\mathbf{2}^{\bullet})/\rho(\mathbf{3}^{\bullet})$=0.98, obtained from Eqs. 7b and 8b.

3.5. Rate constants of CR processes evaluated by using Miller's equation

As described above, differences exist in the TL intensities of ^{3}**2a**–**f**••*,[26] which should be proportional to the product of the generation rate constant and the fluorescence quantum yields (Φ_F) for ^{3}**2a**–**f**••*. The Φ_F values for ^{3}**2a**–**f**••* cannot be determined since temperature is continuously changing through out the entire annealing process in the TL experiments.[27] Therefore, the experimental results can only provide indirect information about the rate constants (k_{CR}) for generation of ^{3}**2a**–**f**••* via CR between **2**•$^+$ and **1**•$^-$, which can be discussed in the context of the schematic energy diagram for the TL (Fig. 6). The TL mechanism proceeds through seven different states (i–vii) and CR between **2**•$^+$ and **1**•$^-$ can occur via four possible exergonic paths (A, B, C, and D in Fig. 6). Only path B, which gives rise to state (iv) ^{3}**2**••*+**1**, is involved in the TL of ^{3}**2**••*.

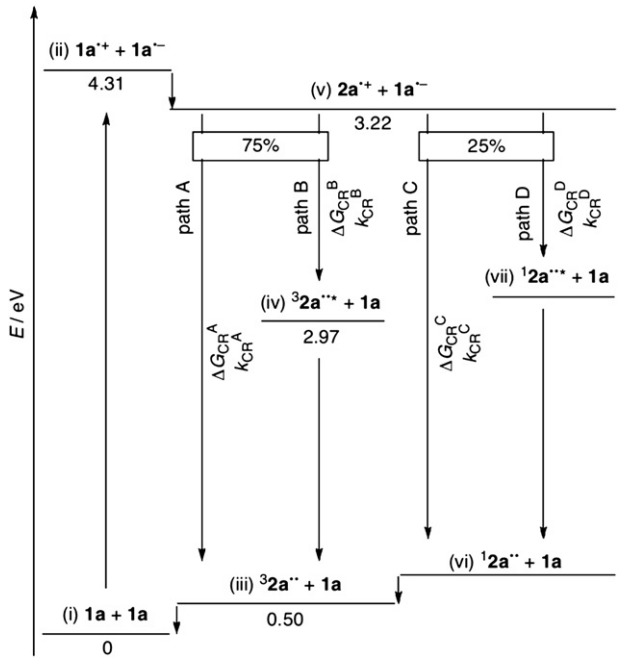

Fig. 6. A schematic energy diagram consisting seven states (i–vii) for four possible paths A–D of CR between $\mathbf{2}^{\bullet+}$ and $\mathbf{1}^{\bullet-}$. The energy values in the diagram are derived from analysis of the parent system ($\mathbf{1a}/^{3}\mathbf{2a}^{\bullet\bullet*}$) and are given in eV.

ΔG_{CR}, associated with paths A and B (ΔG_{CR}^{A} and ΔG_{CR}^{B}) and determined by analysis of the energy diagram and exemplified in Fig. 6 for the parent system $\mathbf{1a}/^{3}\mathbf{2a}^{\bullet\bullet*}$, were found to be −2.72 and −0.25 eV, respectively. ΔG_{CR}^{A} and ΔG_{CR}^{B} for the other derivatives are summarized in Table 3.[26]

If k_{CR} associated with $\mathbf{2}^{\bullet+}$ and $\mathbf{1}^{\bullet-}$ at 135 K is well described by a properly parameterized Eq. 9, a bell-shaped relationship between log k_{CR} and ΔG_{CR} should exist (see Fig. 7). The results obtained by using Eq. 9 suggest that CR between $\mathbf{2a}^{\bullet+}$ and $\mathbf{1a}^{\bullet-}$ that involves generation of $^{3}\mathbf{2a}^{\bullet\bullet*}$ (paths B) is the minor process, as compared with that of $^{3}\mathbf{2a}^{\bullet}$ (paths A). The respective $k_{CR}^{A}(\mathbf{a})$ and $k_{CR}^{B}(\mathbf{a})$ values are 1.8×10^{7} and 1.4×10^{5} s^{-1}, showing that the generation ratio of $^{3}\mathbf{2a}^{\bullet\bullet*}$ and $^{3}\mathbf{2a}^{\bullet\bullet}$ [$k_{CR}^{B}(\mathbf{a})/k_{CR}^{A}(\mathbf{a})$] is 7.7×10^{-3} (Table 3).

On the other hand, the corresponding values of the couple $\mathbf{1c}/^{3}\mathbf{2c}^{\bullet\bullet*}$ are $k_{CR}^{A}(\mathbf{c})=6.8\times10^{7}$ s^{-1} and $k_{CR}^{B}(\mathbf{c})=1.3\times10^{3}$ s^{-1}, showing that generation ratio of $^{3}\mathbf{2c}^{\bullet\bullet*}$ and $^{3}\mathbf{2c}^{\bullet\bullet}$ [$k_{CR}^{B}(\mathbf{c})/k_{CR}^{A}(\mathbf{c})$] is 1.9×10^{-5}. If the amount of $\mathbf{2}^{\bullet+}$ and $\mathbf{1}^{\bullet-}$ formed in systems $\mathbf{1a}/^{3}\mathbf{2a}^{\bullet\bullet*}$ and $\mathbf{1c}/^{3}\mathbf{2c}^{\bullet\bullet*}$ and the Φ_{F} of $^{3}\mathbf{2a}^{\bullet\bullet*}$ and $^{3}\mathbf{2c}^{\bullet\bullet*}$ are nearly the same, the comparison of the k_{CR}^{B}/k_{CR}^{A} ratio between the $\mathbf{1a}/^{3}\mathbf{2a}^{\bullet\bullet*}$ and $\mathbf{1c}/^{3}\mathbf{2c}^{\bullet\bullet*}$ systems means that the TL intensity of $^{3}\mathbf{2c}^{\bullet\bullet*}$ is 400 ($\sim7.7\times10^{-3}/1.9\times10^{-5}$) times smaller than that of $^{3}\mathbf{2a}^{\bullet\bullet*}$. These findings are not inconsistent with the results depicted in Fig. 2. Thus, the differences in TL intensities among $^{3}\mathbf{2}^{\bullet\bullet}$ derivatives are seems to be governed by k_{CR}^{A} and k_{CR}^{B}.

However, similar kinetic analyses of the systems comprised of the couples $\mathbf{1d}$–$\mathbf{f}/^{3}\mathbf{2d}$–$\mathbf{f}^{\bullet\bullet*}$ do not explain the finding that the TLs of $^{3}\mathbf{2d}$–$\mathbf{f}^{\bullet\bullet*}$ are more intense than that of $^{3}\mathbf{2c}^{\bullet\bullet*}$. Errors associated with

Table 3
Free energy changes of CR paths, emission energies, and rate constants of CR at 135 K

Systems	X	$E_{1/2}^{OX}(\mathbf{1})$[a] V	$E_{1/2}^{RED}(\mathbf{1})$[b] V	$E_{1/2}^{OX}(\mathbf{3}^{\bullet})$ V	$E_{EM}(^{3}\mathbf{2}^{\bullet\bullet*})$[c] eV	$\Delta E(^{3}\mathbf{2}^{\bullet\bullet})$ eV	ΔG_{CR}^{A} eV	ΔG_{CR}^{B} eV	k_{CR}^{A} s^{-1}	k_{CR}^{B} s^{-1}	k_{CR}^{B}/k_{CR}^{A}
$\mathbf{1a}/^{3}\mathbf{2a}^{\bullet\bullet*}$	H	+1.82	−2.49	+0.23[d]	2.47	+0.50	−2.72	−0.25	1.8×10^{7}	1.4×10^{5}	7.7×10^{-3}
$\mathbf{1b}/^{3}\mathbf{2b}^{\bullet\bullet*}$	CH_3	+1.65	−2.46	(+0.12)[e]	2.40	+0.48	(−2.58)	(−0.18)	(2.1×10^{7})	(1.7×10^{4})	(8.1×10^{-4})
$\mathbf{1c}/^{3}\mathbf{2c}^{\bullet\bullet*}$	CH_3O	+1.35	−2.51	−0.06[d]	2.34	+0.46	−2.45	−0.11	6.8×10^{7}	1.3×10^{3}	1.9×10^{-5}
$\mathbf{1d}/^{3}\mathbf{2d}^{\bullet\bullet*}$	F	+1.80	−2.27	(+0.20)[e]	2.46	+0.49	(−2.47)	(−0.01)	(5.7×10^{7})	(2.4×10^{1})	(4.2×10^{-7})
$\mathbf{1e}/^{3}\mathbf{2e}^{\bullet\bullet*}$	Cl	+1.93	−2.11	(+0.27)[e]	2.36	+0.48	(−2.38)	(−0.02)	(1.3×10^{8})	(3.6×10^{1})	(2.8×10^{-7})
$\mathbf{1f}/^{3}\mathbf{2f}^{\bullet\bullet*}$	CF_3	+2.18	−2.01	(+0.46)[e]	2.40	+0.50	(−2.47)	(−0.07)	(5.7×10^{7})	(2.8×10^{2})	(4.9×10^{-6})

[a] Determined with $E_{1/2}^{OX}$ ($=E_{cp}-0.03$ V, vs SCE in CH_3CN) obtained by cyclic voltammetry.
[b] Determined with calibration line [$E_{AB}=1.067\times(E_{1/2}^{OX}-E_{1/2}^{RED})-0.024$].[35]
[c] Obtained by the γ-irradiation method.
[d] Quoted from Ref. 37.
[e] Determined by using the Hammett equation, $E_{1/2}^{OX}(\mathbf{3}^{\bullet})=0.363\sigma^{\bullet+}+0.23$.[26,36] ΔG_{CR}^{A}, ΔG_{CR}^{B} k_{CR}^{A}, k_{CR}^{B}, and k_{CR}^{B}/k_{CR}^{A} determined by using these $E_{1/2}^{OX}(\mathbf{3}^{\bullet})$ values are given in parentheses.

On the other hand, non-radiative paths A, C, and D give rise to states (iii) $^{3}\mathbf{2}^{\bullet\bullet}+\mathbf{1}$, (vi) $^{1}\mathbf{2}^{\bullet\bullet}+\mathbf{1}$, and (vii) $^{1}\mathbf{2}^{\bullet\bullet*}+\mathbf{1}$, respectively. Although these non-radiative paths have been disregarded in many earlier efforts, they have been considered in this work. Unfortunately, it is difficult to estimate accurately the energies of the states (vi) and (vii), which contain two semi-stable species of $^{3}\mathbf{2}^{\bullet\bullet}$, i.e., $^{1}\mathbf{2}^{\bullet\bullet}$ and $^{1}\mathbf{2}^{\bullet\bullet*}$. As a result, in the following discussion, we have only given attention to the generation ratio of $^{3}\mathbf{2}^{\bullet\bullet*}$ and $^{3}\mathbf{2}^{\bullet\bullet}$ by using CR rate constants of paths A and B (k_{CR}^{A} and k_{CR}^{B}), whose sum statistically accounts for 75% of all CR opportunities.[30]

From the free energy change of each CR process (ΔG_{CR}), it is possible to determine k_{CR}[29] by using Miller's equation[31a,32] (Eq. 9), which comes from Marcus theory.[31b–e] Note that Eq. 9 does not take into account multiplicities and intersystem crossing and only considers substituents effects on ΔG_{CR}.[34]

$$k_{CR}=\left(\frac{4\pi^{3}}{h^{2}\lambda_{s}k_{b}T}\right)^{1/2}|V|^{2}\sum_{\omega=0}^{\infty}\left(\frac{e^{-s}S^{\omega}}{\omega!}\right)\exp\left\{-\frac{(\lambda_{s}+\Delta G_{CR}+\omega h\nu)^{2}}{4\lambda_{s}k_{b}T}\right\}$$

$$S=\lambda_{v}/h\nu \qquad (9)$$

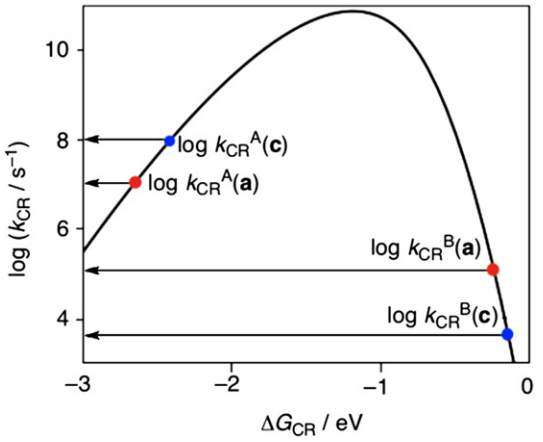

Fig. 7. A bell-shaped relationship of log k_{CR} versus ΔG_{CR} in CR between $\mathbf{2}^{\bullet+}$ and $\mathbf{1}^{\bullet-}$ using a parameterized Eq. 9 given Ref. 32 (135 K). Red and blue dots refer to $\mathbf{1a}/^{3}\mathbf{2a}^{\bullet\bullet*}$ and $\mathbf{1c}/^{3}\mathbf{2c}^{\bullet\bullet*}$ systems, respectively.

E^{RED}(**1**) determined with calibration line, E^{OX}(**3d**–**f**•) determined by using the Hammett equation, parameters in MCH are possible reasons for this deviation, as well as decompositions of $\mathbf{2}^{\bullet+}$ and $\mathbf{1}^{\bullet-}$. As a matter of fact, Φ_F of $^3\mathbf{2}^{\bullet\bullet*}$ is also an important factor in determining TL intensities.

4. Conclusion

In the study described above, we experimentally determined the effects of substituents on TL and PL energies of ^{3}**2a**–**f**••* and **3a**–**f**•* and calculated the ETs of ^{3}**2a**–**f**•• and **3a**–**f**•. Hammett analyses using $\sigma^{\bullet}$ (Cheng) constants showed that substituents have nearly the same effects on the TL and PL energies of ^{3}**2a**–**f**••* and **3a**–**f**•*. The results suggest that $^3\mathbf{2}^{\bullet\bullet*}$ has a largely twisted molecular geometry and a considerably localized electronic structure containing the diarylmethyl radical (subunit I) fluorophore. The results of DFT calculations also provide support for this interpretation. As compared with the TL wavelengths of *gem*-methylphenyltrimethylenemethane (λ_{TL}=461 nm) and *gem*-(2-naphthyl)phenyltrimethylenemethane (λ_{TL}=607 nm),[10a] relatively small but finite changes in TL wavelengths take place when EDGs and/or EWGs are introduced into ^{3}**2a**••* (λ_{TL}=501 nm). Therefore, EDGs and/or EWGs can be employed to fine tune of TL wavelengths. Although induced by either γ- or X-irradiation of **1**, some derivatives of $^3\mathbf{2}^{\bullet\bullet*}$ exhibit very weak or no TL under the X-irradiation conditions. X-irradiation is a convenient method for generating transients for TL measurements, while γ-irradiation is also a powerful method but it requires severe conditions.

Substituents on benzene rings of ^{3}**2a**••* not only affect TL wavelengths but also their intensities, which are controlled mainly by the rate constant ratio $k_{CR}{}^{B}/k_{CR}{}^{A}$ and Φ_F. Thermodynamic and kinetic analyses employing Miller's equation revealed that the radiative path B is inefficient as compared with non-radiative path A ($k_{CR}{}^{B}/k_{CR}{}^{A}<10^{-2}$).

In future efforts, we plan to determine Φ_F of $^3\mathbf{2}^{\bullet\bullet*}$ to complete the analysis of the CR process and gain a fundamental insight into the TL phenomena and its application to ORLED.

Acknowledgements

This study was supported by the Cooperation for Innovative Technology and Advanced Research in Evolutional Area (CITY AREA) program by the Ministry of Education, Culture, Sports, Science and Technology (MEXT), Japan. H.I. gratefully acknowledges financial support in the form of a Grant-in-Aid for Scientific Research on Priority Areas 'New Frontiers in Photochromism' (Nos. 20044027 and 21021025 in the Area No. 471) and Innovative Areas 'π-Space' (Nos. 21108520 and 23108718 in the Area No. 2007), the Scientific Research (B) (Nos. 20044027 and 23350023), and the Challenging Exploratory Research (No. 21655016) from the MEXT of Japan. K.M. also acknowledges financial support in the form of a Grant in-Aid for the Scientific Research (C) (No. 23550058). Y.M. gratefully acknowledges financial support by the Sasakawa Scientific Research Grant from the Japan Science Society.

Supplementary data

The details of the methods used to prepare substrates, details of energy diagrams for TL of ^{3}**2b**–**f**••*, and computational results for the ground states of **1a**–**f**, ^{3}**2a**–**f**••, and **3a**–**f**•are given in the Supplementary data. Supplementary data associated with this article can be found, in the online version, at doi:10.1016/j.tet.2011.06.052.

References and notes

1. (a) Hammett, L. P. *J. Am. Chem. Soc.* **1937**, *59*, 96–103; (b) Hammett, L. P. *Physical Organic Chemistry*, 2nd ed; McGraw-Hill: New York, NY, 1970.
2. (a) Samori, S.; Tojo, S.; Fujitsuka, M.; Spitler, E. L.; Haley, M. M.; Majima, T. *J. Org. Chem.* **2008**, *73*, 3551–3558; (b) Imoto, M.; Ikeda, H.; Ohashi, M.; Takeda, M.; Tamaki, A.; Taniguchi, H.; Mizuno, K. *Tetrahedron Lett.* **2010**, *51*, 5877–5880; (c) Kitamura, C.; Tsukuda, H.; Yoneda, A.; Kawase, T.; Kobayashi, T.; Naito, H. *Eur. J. Org. Chem.* **2010**, 3033–3040; (d) Maeda, H.; Ishida, H.; Inoue, Y.; Merpuge, A.; Maeda, T.; Mizuno, K. *Res. Chem. Intermed.* **2009**, *35*, 939–948; (e) Liddle, B. J.; Silva, R. M.; Morin, T. J.; Macedo, F. P.; Shukla, R.; Lindeman, S. V.; Gardinier, J. R. *J. Org. Chem.* **2007**, *72*, 5637–5646.
3. (a) Fossey, J.; Lefort, D.; Sorba, J. *Free Radicals for Organic Chemistry*; John: West Sussex, 1995; (b) Parsons, A. F. *An Introduction to Free Radical Chemistry*; Wiley-Blackwell: Hoboken, NJ, 2000.
4. Wen, Z.; Li, Z.; Shang, Z.; Cheng, J.-P. *J. Org. Chem.* **2001**, *66*, 1466–1472.
5. Dust, J. M.; Arnold, D. R. *J. Am. Chem. Soc.* **1983**, *105*, 1221–1227.
6. (a) Creary, X. *Acc. Chem. Res.* **2006**, *39*, 761–771; (b) Creary, X.; Mehrsheikh-Mohammadi, M. E.; McDonald, S. *J. Org. Chem.* **1987**, *52*, 3254–3263.
7. Hicks, R. *Stable Radicals: Fundamental and Applied Aspects of Odd-Electron Compounds*; John: West Sussex, 2010.
8. Lv, X.; Mao, J.; Liu, Y.; Huang, Y.; Ma, Y.; Yu, A.; Yin, S.; Chen, Y. *Macromolecules* **2008**, *41*, 501–503.
9. (a) Nishide, H.; Iwasa, S.; Pu, Y.-J.; Suga, T.; Nakahara, K.; Satoh, M. *Electrochim. Acta* **2004**, *50*, 827–831; (b) Nishide, H.; Oyaizu, K. *Science* **2008**, *319*, 737–738.
10. (a) Namai, H.; Ikeda, H.; Hoshi, Y.; Kato, N.; Morishita, Y.; Mizuno, K. *J. Am. Chem. Soc.* **2007**, *129*, 9032–9036; (b) Ikeda, H. *J. Photopolym. Sci. Technol.* **2008**, *21*, 327–332; (c) Ikeda, H.; Matsui, Y.; Akimoto, I.; Kan'no, K.-i; Mizuno, K. *Aust. J. Chem.* **2010**, *63*, 1342–1347.
11. (a) Namai, H.; Ikeda, H.; Kato, N.; Mizuno, K. *J. Phys. Chem. A* **2007**, *111*, 4436–4442; (b) Ikeda, H.; Namai, H.; Kato, N.; Ikeda, T. *Tetrahedron Lett.* **2006**, *47*, 1857–1860.
12. X-irradiation under conditions that are similar to those employed in γ-irradiation provided very weak TL upon annealing.
13. Dunning, T. H. *J. Chem. Phys.* **1989**, *90*, 1007–1023.
14. Becke, A. D. *J. Chem. Phys.* **1993**, *98*, 5648–5652.
15. Lee, C.; Yang, W.; Parr, R. G. *Phys. Rev. B* **1988**, *37*, 785–789.
16. Although the wavelengths of ETs calculated with TDDFT do not always exactly match with values obtained experimentally owing to errors of the excitation energies involved with ground states and excited states that have charge-transfer character, they are sufficiently accurate to enable qualitative analyses. See Ref. 17.
17. Dreuw, A.; Head-Gordon, D. *J. Am. Chem. Soc.* **2004**, *126*, 4007–4016.
18. Frisch, M. J.; Trucks, G. W.; Schlegel, H. B.; Scuseria, G. E.; Robb, M. A.; Cheeseman, J. R.; Zakrzewski, V. G.; Montgomery, J. A., Jr.; Stratmann, R. E.; Burant, J. C.; Dapprich, S.; Millam, J. M.; Daniels, A. D.; Kudin, K. N.; Strain, M. C.; Farkas, O.; Tomasi, J.; Barone, V.; Cossi, M.; Cammi, R.; Mennucci, B.; Pomelli, C.; Adamo, C.; Clifford, S.; Ochterski, J.; Petersson, G. A.; Ayala, P. Y.; Cui, Q.; Morokuma, K.; Malick, D. K.; Rabuck, A. D.; Raghavachari, K.; Foresman, J. B.; Cioslowski, J.; Ortiz, J. V.; Stefanov, B. B.; Liu, G.; Liashenko, A.; Piskorz, P.; Komaromi, I.; Gomperts, R.; Martin, R. L.; Fox, D. J.; Keith, T.; Al-Laham, M. A.; Peng, C. Y.; Nanayakkara, A.; Gonzalez, C.; Challacombe, M.; Gill, P. M. W.; Johnson, B. G.; Chen, W.; Wong, M. W.; Andres, J. L.; Head-Gordon, M.; Replogle, E. S.; Pople, J. A. *Gaussian 98, revision A.11.4*; Gaussian: Pittsburgh, PA, 1998.
19. Stephens, P. J.; Devlin, F. J.; Chabalowski, C. F.; Frisch, M. J. *J. Phys. Chem.* **1994**, *98*, 11623–11627.
20. (a) Ikeda, H.; Hoshi, Y.; Namai, H.; Tanaka, F.; Goodman, J. L.; Mizuno, K. *Chem.—Eur. J.* **2007**, *13*, 9207–9215; (b) Ikeda, H.; Takasaki, T.; Takahashi, Y.; Konno, A.; Matsumoto, M.; Hoshi, Y.; Aoki, T.; Suzuki, T.; Goodman, J. L.; Miyashi, T. *J. Org. Chem.* **1999**, *64*, 1640–1649; (c) Ikeda, H.; Minegishi, T.; Abe, H.; Konno, A.; Goodman, J. L.; Miyashi, T. *J. Am. Chem. Soc.* **1998**, *120*, 87–95.
21. Murov, L. S.; Carmichael, I.; Hug, G. L. *Handbook of Photochemisty*, 2nd ed.; Marcel Dekker: New York, NY, 1993.
22. The broad TL spectrum of $^3\mathbf{2c}^{\bullet\bullet*}$ (Fig. 2c) was deconvoluted into four bands (blue, purple, red, and yellow). The shortest band maximum is listed in the Table 1.
23. Namai, H.; Ikeda, H.; Hoshi, Y.; Mizuno, K. *Angew. Chem., Int. Ed.* **2007**, *46*, 7396–7398.
24. Note that intramolecular orbital interactions likely take place in $^1\mathbf{10}^{\bullet\bullet*}$ but that intramolecular charge-transfer interactions are not expected owing to the fact that $^1\mathbf{10}^{\bullet\bullet*}$ contains essentially the same two radical moieties.
25. Fig. 4 was drawn with WinMOPAC 3.9; Fujitsu Ltd.: Tokyo, Japan, 2004.
26. For the detail, see the Supplementary data.
27. Determinations of Φ_F for short-lived intermediates at room temperature have been carried out by Majima and co-workers,[28] by using multi-laser flash photolysis spectroscopy. Studies leading to the determinations of Φ_F for ^{3}**2a**–**f**••* employing a similar methodology will be reported elsewhere.
28. (a) Oseki, Y.; Fujitsuka, M.; Sakamoto, M.; Majima, T. *J. Phys. Chem. A* **2007**, *111*, 9781–9788; (b) Sakamoto, M.; Cai, X.; Kim, S. S.; Fujitsuka, M.; Majima, T. *J. Phys. Chem. A* **2007**, *111*, 223–229; (c) Cai, X.; Tojo, S.; Fujitsuka, M.; Majima, T. *J. Phys. Chem. A* **2006**, *110*, 9319–9324; (d) Ouchi, A.; Li, Z.; Sakuragi, M.; Majima, T. *J. Am. Chem. Soc.* **2003**, *125*, 1104–1108.
29. We have not considered the dissociations of [$\mathbf{2}^{\bullet+}$/$\mathbf{1}^{\bullet-}$] to the corresponding free ions.
30. Helfrich, W.; Schneider, W. G. *Phys. Rev. Lett.* **1965**, *14*, 229–232.
31. (a) Miller, J. R.; Beitz, J. V.; Huddleston, R. K. *J. Am. Chem. Soc.* **1984**, *106*, 5057–5068; (b) Siders, P.; Marcus, R. A. *J. Am. Chem. Soc.* **1981**, *103*, 741–747; (c) Siders, P.; Marcus, R. A. *J. Am. Chem. Soc.* **1981**, *103*, 748–752; (d) VanDuyne, R.

P.; Fischer, S. F. *Chem. Phys.* **1974**, *5*, 183–197; (e) Ulstrup, J.; Jortner, J. *J. Chem. Phys.* **1975**, *63*, 4358–4368.
32. In Eq. 9, V, λ_s, λ_v, ν, and ΔG_{CR} are an electronic coupling matrix element (V=18 cm^{-1}), solvent reorganization energy (λ_s=1.00 eV), vibration reorganization energy (λ_v=0.25 eV), single average frequency (ν=1500 cm^{-1}), and free energy change for CR process (ΔG_{CR}), respectively. In addition, h, k_b, and T are Planck's constant, Boltzmann's constant, and temperature, respectively. The experimental parameters were determined by Kikuchi and co-workers[33] for a variety of benzene derivatives in dichloromethane, and were used.
33. Niwa, T.; Kikuchi, K.; Matsushita, N.; Hayashi, M.; Katagiri, T.; Takahashi, Y.; Miyashi, T. *J. Phys. Chem.* **1993**, *97*, 11960–11964.
34. Actually, introduction of the substituents will not only affect ΔG_{CR} but also λ_s, λ_v, and other parameters.
35. The E^{RED} values of **1a**–**f** were estimated with the calibration line [E^{AB}= 1.067×($E_{1/2}{}^{OX}$–$E_{1/2}{}^{RED}$)–0.024] obtained by using E^{OX} and absorption energy (E_{AB}) of **1a**–**f**.[10a]
36. (a) Wayner, D. D. M.; McPhee, D. J.; Griller, D. *J. Am. Chem. Soc.* **1988**, *110*, 132–137; (b) Sim, B. A.; Milne, P. H.; Griller, D.; Wayner, D. D. M. *J. Am. Chem. Soc.* **1990**, *112*, 6635–6638; (c) Workentin, M. S.; Wayner, D. D. M. *Res. Chem. Intermed.* **1993**, *19*, 777–785.
37. Ikeda, H.; Akiyama, K.; Takahashi, Y.; Nakamura, T.; Ishizaki, S.; Shiratori, Y.; Ohaku, H.; Goodman, J. L.; Houmam, A.; Wayner, D. D. M.; Tero-Kubota, S.; Miyashi, T. *J. Am. Chem. Soc.* **2003**, *125*, 9147–9157.